ORIGINAL PAPER

Hurricane flood risk assessment for the Yucatan and Campeche State coastal area

Wilmer Rey[1,2] · E. Tonatiuh Mendoza[2,3] · Paulo Salles[2,3] · Keqi Zhang[4] · Yi-Chen Teng[5,6] · Miguel A. Trejo-Rangel[2] · Gemma L. Franklin[2,3]

Abstract

In this study, the first ever Sea, Lake, Overland Surges from Hurricanes (SLOSH) grid was built for the Yucatan Peninsula. The SLOSH model was used to simulate storm surges in the coastal area of the states of Yucatan and Campeche (Mexico). Based on climatology, more than 39,900 hypothetical hurricanes covering all possible directions of motion were synthesized. The storm intensity (category), forward speed, radius of maximum winds and the tide anomaly were varied for each hypothetical track. According to these scenarios, the potential storm surge and associated inundation threat were computed. Subsequently, the Maximum Envelope of Water (MEOW) and the Maximum of the MEOWs (MOMs) were calculated to assess the flood hazard induced by tropical cyclones under varying conditions. In addition, for each MOM, the socioeconomic vulnerability aspects were taken into account in order to assess the hurricane flood risk for the states of Yucatan and Campeche. Results show that the most vulnerable areas are the surroundings of Terminos lagoon, Campeche City and its neighboring areas in the state of Campeche. For Yucatan, the towns located in the Northwest (Celestun, Hunucma and Progreso) and the eastern part of the state presented the highest risk values. The methodology used in this study can be applied to other coastal zones of Mexico as well as places with similar attributes. Furthermore, the MEOW and MOM are very useful as a decision-making tool for prevention, preparedness, evacuation plans, mitigation of the flood hazard and its associated risk, and also for insurance companies.

Keywords Flood modeling · Flood hazard · Flood vulnerability · Flood risk · MEOW · Yucatan Peninsula

1 Introduction

Due to its geographical position, characteristic low-lying coast and wide continental shelf, the northern part of the Yucatan Peninsula is susceptible to flooding during events such as the Central American Cold Surge, locally called Nortes (Appendini et al. 2018;

✉ Wilmer Rey
   w.reysanchez@gmail.com

Extended author information available on the last page of the article

Rey et al. 2018) and tropical cyclones (TCs). It is important to assess the inundation threat, given the severity of the effects of TC events. For instance, according to El Diario de Yucatan (DY 1988) a local newspaper, Hurricane Gilbert in 1988 caused approximately $103 million USD in losses, and affected 400,000 people, with 10 fatalities at Progreso port. Hurricane Isidore hit the Peninsula in 2002, causing 11 deaths. These events have a low occurrence along the northern Yucatan coast, on average only 0.16 events per year (Rosengaus-Moshinsky et al. 2002). In this sense, there is a lack of historical hurricane databases to assess the inundation threat from historical hurricanes in this zone. Even though there is no detectable trend in the global annual frequency of TCs in historical cyclone data, net power dissipation is a better indicator than storm frequency, and has shown an increase over the past 30 years because either the storms have become more intense or have survived at high intensity for a longer period of time (Emanuel 2005). This indicator is highly correlated with the tropical Atlantic sea surface temperature (Knutson 2015). Therefore, even when the annual frequency of TCs is low, the intensity may be higher for future climate projections (Knutson et al. 2010; Knutson 2015). In addition, a regional study reported an increasing trend in the frequency of TCs, especially in the Mexican Caribbean Sea (Ojeda et al. 2017). The limitations of historical tropical cyclone data to evaluate the inundation threat at specific sites has been solved by the use of synthetic (Emanuel et al. 2006, 2008) or hypothetical (Zachry et al. 2015) hurricanes. These provide more robust data sets for statistical analysis in order to characterize present and future climate trends as well as for evacuation planning.

Most of the effects caused by flooding induced by extreme storms are largely due to storm surges, i.e., the rise of the seawater level generated by a storm, over and above the predicted astronomic tide (NHC 2014a). Storm surges are mainly generated by wind shear stress on the sea surface and the presence of a land mass (coast) downwind, especially in shallow waters in the coastal zone (Flather 2001), as well as perturbations in atmospheric pressure (Lin and Chavas 2012), which are relatively small compared to wind stress on the sea surface. The rule of thumb is that for every 1-mb drop in pressure, there is a 1-cm rise in ocean surface (Massey et al. 2007). The storm surge may also be affected by interaction with seiches in semi-enclosed basins, the storm size and forward speed, as well as the direction and duration of the incident wind (Rey et al. 2018). This phenomenon is not fully understood by most people living in coastal regions, therefore the public awareness of flood hazard is unfortunately low. In this regard, if these episodes are presented in a map showing the extent of flooding and the water depth (i.e., water level above the terrain or difference between flood level and the terrain), it becomes quite easy to understand for the general public (Zachry et al. 2015). Morrow et al. (2015) stated that visualizations, such as inundation maps defining four levels of surge threat with different colors, are an effective communication tool for helping the society to understand the storm surge warning. However, visualization of the flood hazard, though useful and necessary, is not sufficient for decision making. In order to exhibit the consequences of floods on society, urban development and natural environments, the hazard map has to be used in combination with the vulnerability map to determine the flood risk, which offers additional tools for flood risk management (Plate 2002; Merz et al. 2007; Dinh et al. 2012).

The aim of this paper is to assess the hurricane flood risk for the states of Yucatan and Campeche, Mexico, by means of a quantitative assessment of floods caused by events ranging from tropical storms to category-V hurricanes, based on the Saffir–Simpson Hurricane Wind Scale (SSHWS), together with socioeconomic vulnerability indicators. In this sense, this study provides a qualitative assessment of the societal impacts caused by flooding due

to hurricanes. The methodology used may be applied to other sites around the world with the same features.

2 Theoretical considerations

Risk management has been discussed by means of several terms, including risk, hazard, vulnerability, exposure, susceptibility and resilience (Merz et al. 2010). Given that there is still no consensus on most of these terms (Gallopín 2006; Cutter et al. 2008), it is necessary to define the terms used in this study. While hazard is defined as a phenomenon or human activity that may cause loss of life, injury or other health impacts, property damage, social and economic disruption or environmental degradation (International Strategy for Disaster Reduction, UNISDR 2009), vulnerability is defined as a measure of the intrinsic susceptibility of an element exposed to a potentially damaging natural phenomena (Tingsanchali and Karim 2005), either a long-term stressor or a short-term intense shock. Vulnerability consists of two elements, exposure and susceptibility; the former is quantified by the number of elements at risk (damage potential), and the latter provides the degree of damage (loss) to the element exposed to the hazard. Vulnerability comprises several sectors including social, economic, institutional and environmental aspects as well as infrastructure resilience (Cutter et al. 2008; Nageswara Rao et al. 2008; UNISDR 2009; Merz et al. 2010; Balica et al. 2013). Flood hazard depends on many factors such as water depth, flow velocity, storm duration, the rate of water rise for the overland flow and flow frequency (Dinh et al. 2012). However, different studies have identified water depth as the flood characteristic with the strongest influence on flood damage (Penning-Rowsell et al. 1994; Wind et al. 1999). Flood risk is defined as the product of the hazard factor and the vulnerability factor for each land unit (Plate 2002; Bronstert 2003; Tingsanchali and Karim 2005; Dinh et al. 2012), considering not only the direct economic damage but also the adverse consequences of the flood on the population in the flood-prone area (Merz et al. 2007).

Flood risk assessment studies in the Yucatan Peninsula are scarce. However, worldwide there are several studies on this topic, some of which include the effects on the population (Chowdhury and Karim 1996; Tingsanchali and Karim 2005), while others take into account additional effects, such as: social, environmental and spatial dynamics, referring to the ability of people to cope with hazards (Clark et al. 1998); hydrogeological, socioeconomic and political-administrative components (Dinh et al. 2012); and physical aspects (Nageswara Rao et al. 2008; Balica et al. 2013; Martínez-Graña et al. 2016; Di Risio et al. 2017; Silva et al. 2017; Ruol et al. 2018).

In Mexico, there is a methodology used at a federal level to assess the flood risk induced mainly by TCs (Cenapred 2006). However, it is focused only on economical assets and lacks the accountability of other vulnerability dimensions such as social, institutional, ecological and cultural aspects, which are important to consider.

3 Methodology

The development of the flood risk assessment covers three main aspects: Sect. 3.1 (Hazard Characterization), which comprises the use of the hydrodynamic SLOSH (Sea, Lake, Overland Surges from Hurricanes) model (Jelesnianski et al. 1992), Sect. 3.2 (Socioeconomic vulnerability) assessment using 17 indicators with municipality spatial resolution,

and Sect. 3.3 (Flood risk assessment), which was obtained by combining the two previously mentioned elements.

Flood hazard was characterized using the SLOSH model, and the vulnerability was characterized with the socioeconomic indicators provided by the National Institute of Geography and Statistics (INEGI 2010).

3.1 Hazard characterization

The SLOSH is a two-dimensional, finite-difference coastal ocean model, developed by the Techniques Development Laboratory of the National Weather Service (Jelesnianski et al. 1992). It is the official model used for over two decades by the National Hurricane Center (NHC) (Massey et al. 2007) to run: (a) real-time operational hurricane storm surge data (Shaffer et al. 1989); (b) hypothetical events for evacuation planning (Zachry et al. 2015); (c) historical events for validation purposes; (d) probabilistic hurricane storm surges (Taylor and Glahn 2008); and (e) extratropical storm surge predictions (Forbes et al. 2014). Initially, only curvilinear, polar coordinate grid systems were employed in SLOSH (Jelesnianski et al. 1992); however, recent developments in the model have introduced elliptical and hyperbolic grids (Massey et al. 2007). These allow finer resolution nearshore (i.e., usually the area of interest) and coarser resolution at the distant boundaries of a large basin (i.e., usually areas of less importance). The computational scheme is formulated on a semi-staggered Arakawa B-grid with velocity components at the four corners of a grid cell and the elevation at the center (Arakawa and Lamb 1977). The SLOSH model computes surges over bays and estuaries, and allows sub-grid scale features such as barriers that impede the flow of the water. These barriers include coastal sand dunes, natural ridges, reefs, levees and other man-made structures that play important roles in reducing or enhancing overland surge flooding. Cuts between barriers must also be included to properly allow for water flow. In addition, deep and narrow channels and rivers with varying widths are incorporated. Therefore, flow through barrier gaps, adverse river flow and deep passes between bodies of water are allowed. Each grid cell must be populated with the average elevation or depth in similar vertical datum, and the surface wind coefficient must be assigned based on land-cover classification data sets. The horizontal transport equations are solved through the application of the Navier–Stokes momentum equations for incompressible and turbulent flow and solved for the pressure, Coriolis and frictional forces every time step. The governing equations are integrated over the entire depth of the water column as derived by Platzman 1963, in which the dissipation is determined solely by an eddy viscosity coefficient, and modified with a bottom slip coefficient proposed by Jelesniansky (1967). The bottom stress is not determined by the depth-averaged velocity. Instead, it is based on a vertical velocity profile that considers the effects of Ekman drift (Jelesnianski 1970; Kim and Chen 1999). Water-level gradients are incorporated, but neither advective acceleration nor horizontal diffusion terms are included in the equation of motion. In addition, overtopping of barrier systems, levees and roads is incorporated. Also, inland inundation is included by means of a wetting and drying algorithm. Given the use of linearized momentum equations, SLOSH is highly computationally efficient, which makes it possible to simulate a large number of hypothetical surge events. The model is forced by surface wind stress and atmospheric pressure drop. At its inception, tides were ignored except for superposition onto the computed surge. However, recent upgrades to the numerical model have included the incorporation of astronomical tides dynamically at every time step and at every SLOSH model grid point to increase accuracy (Taylor et al. 2013). Imbedded with

the SLOSH model is a hurricane wind model. The input parameters of the wind model are the storm track (latitude and longitude of the center's location), radius of the maximum winds and the central pressure drop of the storm. A wind speed profile with respect to the radius from the storm's center is assumed. Corrections to the wind speeds are made for forward storm motion, giving the storm a more accurate asymmetric shape. The accuracy of the predicted surge heights is ±20% when the tropical cyclone is adequately described (Jelesnianski et al. 1992). The limitations of the model are the exclusion of advective acceleration and horizontal diffusion terms in the momentum equation, neglecting the effect of land cover on inundation and insufficient spatial resolution to fully describe the overland flooding (Jelesnianski et al. 1992; Zhang et al. 2013). For more details, readers are referred to Jelesnianski et al (1992).

The computational domain covers the Southeast part of Mexico. The domain was edited at the grid cell level to represent levees, channels, barrier islands and small coastal lagoons. The spatial resolution of the grid along the northern part of the Peninsula varies from 490 to 600 m and from 477 m to 1.6 km for the Campeche coast.

The black polygon in Campeche and the littoral strip along Yucatan in Fig. 1 show the regions where high topographic resolution was available. Along the Yucatan State coast, a 1.6-km-wide strip of LIDAR topographic data with a spatial resolution of 1 m was used. For Campeche, the LIDAR topographic data used has a spatial resolution of 5 m. Gaps in the topography for the entire computational domain were complemented with the ETOPO1 database (Amante and Eakins 2009). The bathymetry was extracted from ETOPO1, and along the Yucatan coast it was complemented with higher-resolution data from 9-km-long
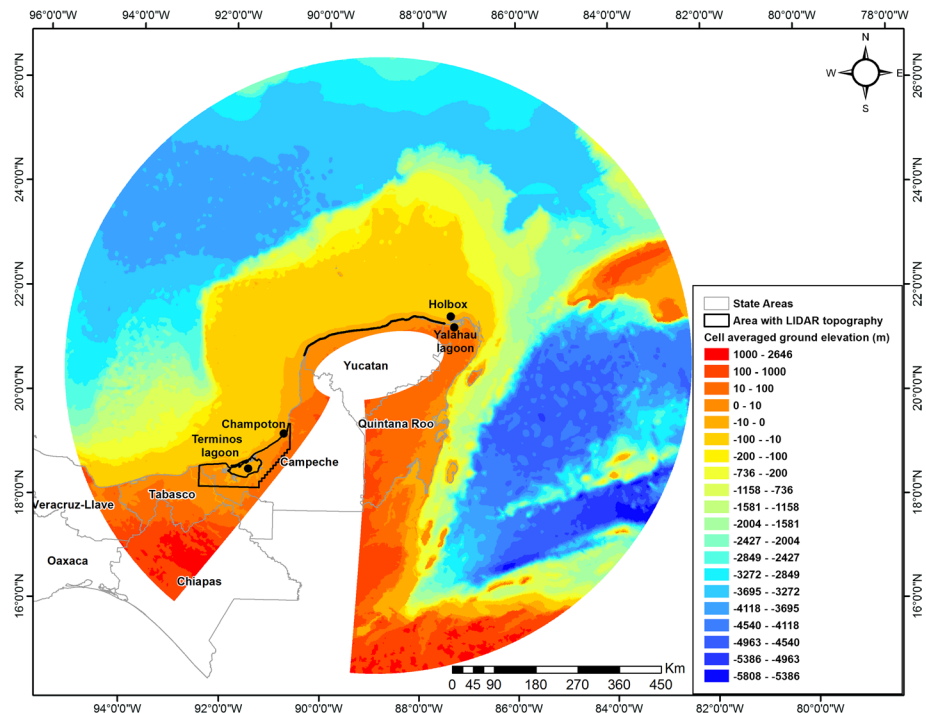

Fig. 1 SLOSH grid (cell-averaged topographic elevation and bathymetric depth)

cross-shore transects every 4 km. The bathymetry used for Campeche was complemented with higher-resolution data for Terminos lagoon and the coastal zone. For the state of Quintana Roo, both the topography and bathymetry were available from ETOPO1 except for Holbox Island where surveys were carried out to collect topographic data for the populated area and bathymetric data for the Yalahau lagoon. Figure 1 shows the SLOSH grid cell average topographic elevation and bathymetric depth; in general, the scarcity of high-resolution topo-bathymetric data is one of the limitations of this study.

The global land-cover classification with 30-m resolution from the National Geomatics Center of China data set (Chen et al. 2015) was used to compute the surface wind stress for each grid cell.

3.1.1 Model validation

One of the main limitations of this study is the lack of hurricane storm surge data to validate the model results. However, during the passage of Hurricane Wilma over Holbox Island (in the state of Quintana Roo) in 2005, a watermark was registered. This mark was used to validate the SLOSH results for that storm event. In addition, a second hydrodynamic model (MIKE 21 HD, in honor of its developer Michael B. Abbott, and 21 because the model has two horizontal dimensions and one vertical dimension) for the entire Gulf of Mexico (Rey et al. 2018) was used to compare hurricane storm surge results. The hydrodynamic module of MIKE 21 is a two-dimensional model developed by the Danish Hydraulic Institute (DHI), based on the finite volume scheme, which resolves the depth-averaged (2D) incompressible Reynolds average Navier–Stokes equations under the Boussinesq and hydrostatic pressure approximation (DHI 2014). The wetting and drying algorithm is included following the work of Zhao et al. (1994) and Sleigh et al. (1998). For more detailed information about the model, readers are referred to the scientific manual documentation (DHI 2014). The computational cost is greater using MIKE 21 than with SLOSH, in part because it solves the continuity and full momentum equations. One of the limitations of MIKE 21 is that the land cover (tree category) is not included to compute surface wind stress at each element, which has an important effect on inundation. When the land cover is taken into account, the inland wind field can be modeled more appropriately and thus provide a better surge simulation (Jelesnianski et al. 1992; Zhang et al. 2008).

The validation consisted of running: the MIKE 21 and SLOSH models without astronomic tide; both hydrodynamic models were forced with wind and pressure fields on the surface, making use of the parametric wind model embedded in the SLOSH model (Jelesnianski et al. 1992) and the storm characteristics from the HURDAT database (Jarvinen et al. 1984). In this sense, only the storm surge was modeled in both models. For the MIKE 21 model, two different boundary conditions were used between Cancun and Cuba and between Cuba and Florida. In this case, the boundaries were set as open (DHI 2014) to generate only storm surge as mentioned above. The inverse pressure-adjusted boundary conditions were used as open boundary conditions for the SLOSH model (Jelesnianski et al. 1992). In this study, the SLOSH version used does not dynamically simulate tides, except for linear superposition onto the computed surge. Therefore, tides were not used as forcing in the SLOSH model for the validation test. However, given the small tidal range along the Yucatan coast, which is from 0.1 m (neap) to 0.8 m (spring) (Cuevas-Jiménez and Euán-Ávila 2009), the astronomical tide contribution to the total water level during the pass of TCs is expected to be low.

The MIKE 21 model with tides; in this case, both boundaries for MIKE 21 were forced with tides from the global tide model (Andersen 1995) to generate storm tide (storm surge plus astronomic tide).

3.1.2 Generation of hypothetical events data set

Hypothetical TCs were created based on the climatology of the study area. Twelve different directions were used to cover possible direction of motion (Fig. 2). For each direction, many parallel tracks were assessed (from 30 to 68 with an approximate distance of 16 km between each of them), based on the orientation and shape of the coast relative to each direction. For each storm track, the storm characteristics varied as follows:

- Two radiuses of maximum wind (RMW, associated with the storm size): 20 miles (32.186 km) and 35 miles (56.327 km),
- Three forward speeds: 5 miles/h (8.04 km/h), 15 miles/h (21.14 km/h) and 25 miles/h (40.23 km/h) and
- Six tropical cyclone categories associated with six pressure gradients: 20 hPa (tropical storm), 28 hPa (hurricane Cat. 1), 40 hPa (Cat. 2), 60 hPa (Cat. 3), 80 hPa (Cat. 4) and 100 hPa (Cat. 5).
- Two tide anomalies were used: low tide (0 m referred to the GGMO6 Mexican geoid) and high tide, equivalent to the mean high water level (MHWL; 0.44 m referred to the GGMO6 Mexican geoid). This MHWL level would provide a more typical level than, for instance, the highest astronomical tide, which would be atypical. On any given day,
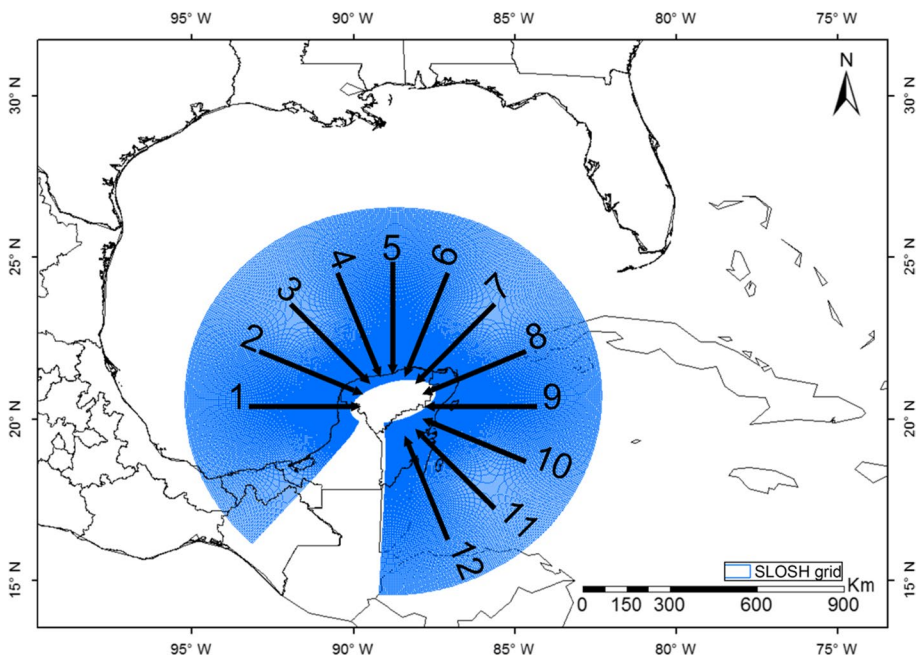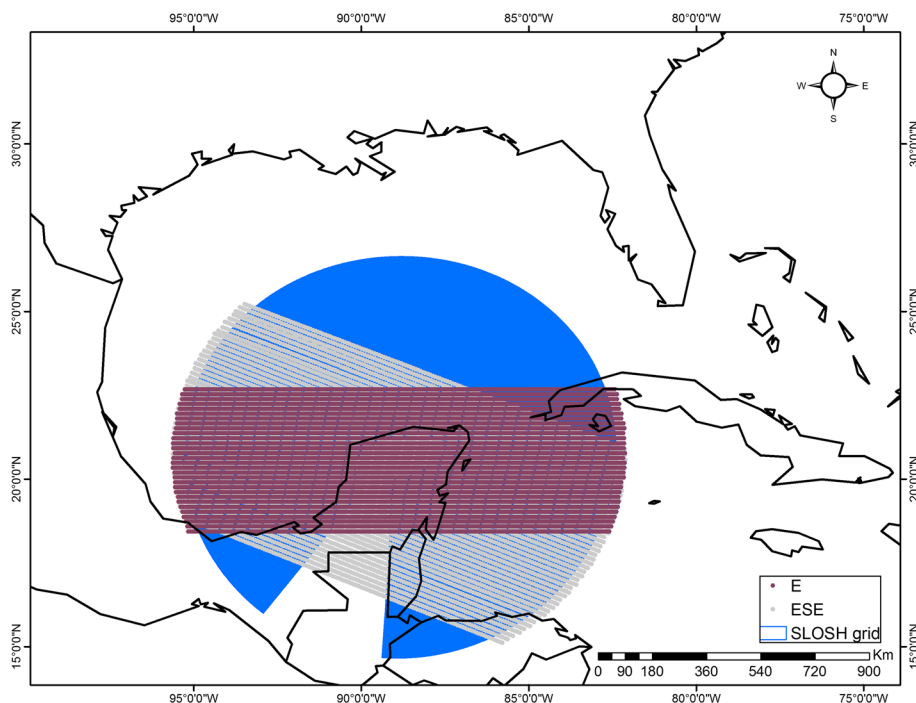

Fig. 2 SLOSH domain and forward directions of motion

Table 1 Number of tracks per direction of motion

Directions	1	2	3	4	5	6	7	8	9	10	11	12
Tracks	30	46	55	59	54	62	68	57	47	50	43	34

Fig. 3 An example of 30 and 46 parallel tracks from the E and ESE direction, respectively

the specific height of the highest tide may be greater or not equal to the mean due in part to other factors. However, the mean would provide a reference level from which naturally occurring fluctuations are removed, thus providing a better representation of the daily high tide.

In other words, for each parallel hurricane track, the storm intensity, forward speed of the storm, radius of maximum winds and the tide anomaly vary.

3.1.3 Generation of MEOWs and MOMs data set

The SLOSH model was run to simulate water level and the inland extent of the flooding caused by individual tracks.

In total, 39,930 TCs were created as a result of 12 different directions with: (i) 30 to 68 parallel storm tracks, as shown in Table 1 (for example, Fig. 3 shows 30 and 46 tracks for directions from the East—**E**—and East-southeast—**ESE**—, respectively); (ii) two radiuses of maximum wind (except for tropical storms where only one radius was used); (iii) three forward speeds; (iv) six storm categories; and (v) two astronomic tide levels.

The SLOSH model was forced with wind and pressure fields from the 39,930 hypothetical cyclones. Subsequently, the hurricane storm surge was obtained for each track, and the maximum envelopes of water (MEOW) were then computed for all of these flood scenarios. The MEOW is composed of the maximum surge at each grid cell computed by the SLOSH model based on a large ensemble of storms of a given category and forward speed with varying sizes, track direction and initial tide level (Shaffer et al. 1989; NHC 2014b). In this sense, each of the 432 computed MEOWs corresponds to one direction of motion (taking into account all parallel tracks associated with that direction), a storm category, a forward speed with two storm sizes (except for tropical storm where only one was applied) and an astronomic tide level. The storm size (related to the RMW) is independent of the MEOW. If at a specific grid cell, the larger RMW produces higher water than the smaller one, that value is retained. As two constant astronomic tide levels were used, 216 MEOWs were obtained for high tide and 216 MEOWS for low tide. Thereafter, the Maximum of the MEOWs (MOMs) were then computed for a given category of hurricanes, showing coastal areas that could be flooded by this category of storms from all directions and forward speeds, and an astronomic tide level (low or high). The MOM provides a worst-case scenario snapshot for a particular storm category under "perfect" storm conditions (NHC 2014c). Hence, six MOMs for high tide and six MOMs for low tide were obtained. The flooded area from a single event is usually less than those from the MEOWs and MOMs corresponding to the category of the event. This is due to the fact that MEOWs and MOMs are used for evacuation plans from a conservative perspective rather than to forecast a single event (Zhang et al. 2013). Due to the coarse resolution of the topographic data used for the state of Quintana Roo, both its MEOWs and MOMs were removed from the database and the study. The water depth for each MEOW and MOM was computed by subtracting the topography high levels from the modeled surface water highs.

3.2 Socioeconomic vulnerability

In order to estimate the vulnerability, an official database of socioeconomic information was used (INEGI 2010). The database is at municipal resolution (smallest political division in Mexico) and contains 306 indicators, of which 17 were taken into account (see Table 2) based on previous studies, which used similar indicators to identify flood vulnerable groups from a socioeconomic perspective (Chen et al. 2013; Cutter et al. 2013; Nkwunonwo et al. 2015; Fernandez et al. 2016). The values of all these indicators were standardized on a scale from 0 to 1, dividing the real value of the indicator by the maximum value of the indicator among all the municipality land units. The same standardization method for indicators of vulnerability has been used in several flood risk assessment studies (Chowdhury and Karim 1996; Tingsanchali and Karim 2005; Dinh et al. 2012). These 17 indictors were divided into two groups. The first group consisted of five indicators (total inhabitants, population under 14 years old, population over 64 years old, illiterate population and disabled population), which represent a weighting of 50% of the vulnerability. The second group is formed by the other 12 indicators, which represent the remaining weighting of 50% of the vulnerability as shown in Table 2. These indicators were weighted based on a discussion among the researchers involved in this study. Thereafter, for each municipality, the 17 indicators were summed in order to obtain a single indicator. The maximum value for each indicator at municipality level is also shown in Table 2.

Table 2 Indicators which were taken into account to estimate socioeconomic vulnerability

INEGI code	Description	Weight	Max
POB1	Total inhabitants	0.10	830,732
POB8	People under 14 years old	0.10	197,729
POB24	People over 64 years old	0.10	59,425
ECO25	Unemployed population	0.04	9794
EDU28	Illiterate population	0.10	20,144
DISC1	Disabled population	0.10	37,549
INDI4	Non-Spanish speaker (indigenous population)	0.04	7782
MIG4	People born in a different entity	0.04	11,871
MIG7	Foreign population	0.04	5200
SALUD2	Population with no health services	0.04	192,997
SCONY7	Divorced or widowed population	0.04	71,704
VIV0	Total private homes	0.04	287,649
VIV1	Total inhabited homes	0.04	229,705
VIV25	Homes with no services (electricity, water, sewer system)	0.04	1088
VIV30	Homes with no fridge, washing machine or car	0.04	9349
VIV40	Homes with no communication technologies (phone, TV, Internet, computer)	0.04	2173
VIV41	Homes with no home appliances (fridge and washing machine)	0.04	1845

3.3 Risk computation

Flood hazard categorization could be defined as a probabilistic function, which describes the magnitude of potential damage by a phenomenon over time (Chowdhury and Karim 1996; Clark et al. 1998; Merz et al. 2007). However, in the absence of flood time series data (as in this study), probabilistic analysis is not possible (Chowdhury and Karim 1996). In this case, the flood hazard categorization can be defined based on the water depth-induced level of difficulties in daily life or damage to properties (Tingsanchali and Karim 2005; Dinh et al. 2012), shown in Table 3. Given that the 12 MOMs for low and high tide do not have an associated return period, they were transformed from water depth into an interval from 0 to 1 to show the spatial distribution of the flood hazard (Merz et al. 2007). The flood hazard categorization in this study is the same as that proposed by Dinh et al. (2012). This categorization was chosen since the study area is low-lying; on average, the Yucatan

Table 3 Food risk categories

Water depth (m)	Hazard	Vulnerability (natural breaks and Jenks)	Flood risk	Hazard/vulnerability/risk zones
0.0–0.2	0.0–0.04	0–0.03	0.0–0.0012	Very low
0.2–0.5	0.04–0.1	0.03–0.08	0.0012–0.008	Low
0.5–1.0	0.1–0.2	0.08–0.13	0.008–0.026	Medium
1.0–2.0	0.2–0.4	0.13–0.34	0.026–0.136	High
>2.0	0.4–1.0	0.34–1.0	0.136–1.0	Very high

Peninsula has an elevation of 10 m above mean sea level (MSL) (Stringfield and LeGrand 1974) and along the northern part of the Yucatan coast the average elevation above MSL is around 2 m (Rey et al. 2018). Therefore, five flood hazard categories were used (Table 3). Regarding the vulnerability categories, the natural breaks method (Jenks 1963) was used to create five categories. This method is used to minimize the squared deviations of the class means. This was applied for all the municipalities since the vulnerability indicators have values from 0 to 0.34, with the exception of Merida with a value of 0.9, which has the largest population, 830,732 inhabitants according to the 2010 National Census demographic data (INEGI 2010). Therefore, when a large population is exposed to a hazard, higher vulnerability is presented (Dinh et al. 2012). The flood risk was calculated as the product of the hazard and vulnerability indicators. Accordingly, the highest flood risk is located in the areas with maximum water depth and highest vulnerability.

4 Results

4.1 Flood hazard assessment

4.1.1 Model validation

Results from the SLOSH and MIKE 21 models show similarities for the maximum storm surge for hurricane Wilma at Holbox Island (Fig. 4). Differences between MIKE 21 and SLOSH for the storm surge at the beginning and at the end of the simulation are mainly due to the different wetting and drying schemes used for each model. The watermark was at 2.4 m, and the storm surge model results reached up to 2.2 m. The difference is partly associated with the contribution of the astronomic tide (blue line), as shown by the MIKE 21 storm tide result (black line), which takes into account the astronomic tide contribution. Consequently, it is assumed that the SLOSH model provides adequate results for the study area. For future studies, the scarcity of sea-level data to validate hydrodynamic models along the Yucatan coast is expected to be solved with the tide gauges that have been
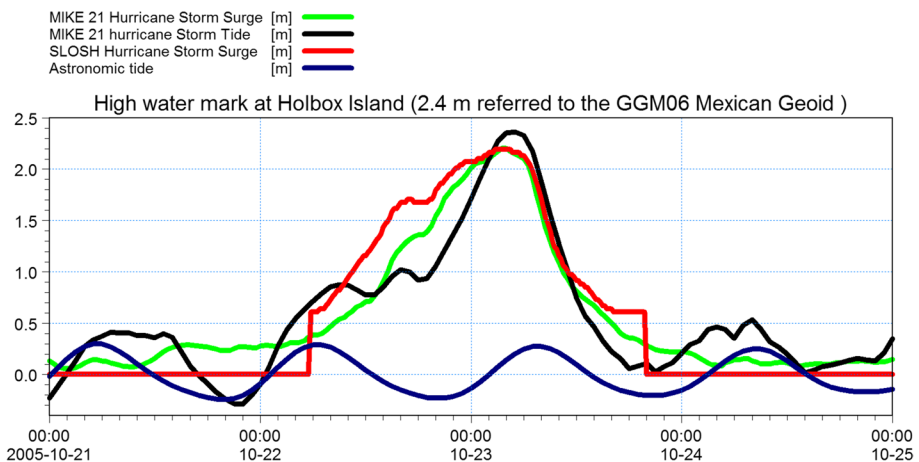

Fig. 4 Hurricane storm surge time series (green and red for MIKE 21 and SLOSH model, respectively); the blue line is the predicted astronomic tide, and the black line is the storm tide

installed in the last decade, a period in which no cyclone has hit the northern coast of the Peninsula. It is important to mention that even if both models reproduce similar results for the storm surge (Fig. 4), the extent of the flooding is not necessarily the same, mainly due to differences in the wetting and drying algorithm, overland bottom friction and including or ignoring nonlinear terms in the equations. The difference in the peak storm surge computed by different hydrodynamic models (with and without nonlinear terms) is usually small for the open ocean and large in shallow bays and lagoons (Zhang et al. 2013).

As an example, the Maximum Envelope of Water at each grid cell induced by hurricane Wilma (2005) along the eastern coast of the Peninsula is shown in Fig. 5. Given the cyclone trajectory (brown points), the shallow water and the geometry of the Yalahau lagoon, the storm surge reached maximum levels around this lagoon. According to both the model and accounts from the local inhabitants, the urban area in Holbox Island was covered by seawater.

4.1.2 MOMs for Yucatan and Campeche State

Hazard MOMs from tropical cyclone up to category-II hurricanes for low and high tide are presented in Fig. 6, and for category-III to category-V hurricanes in Fig. 7. It is necessary to clarify that each MOM map from category I to category V was created based on 3630 storm events, whereas for the tropical storm category each MOM was based on
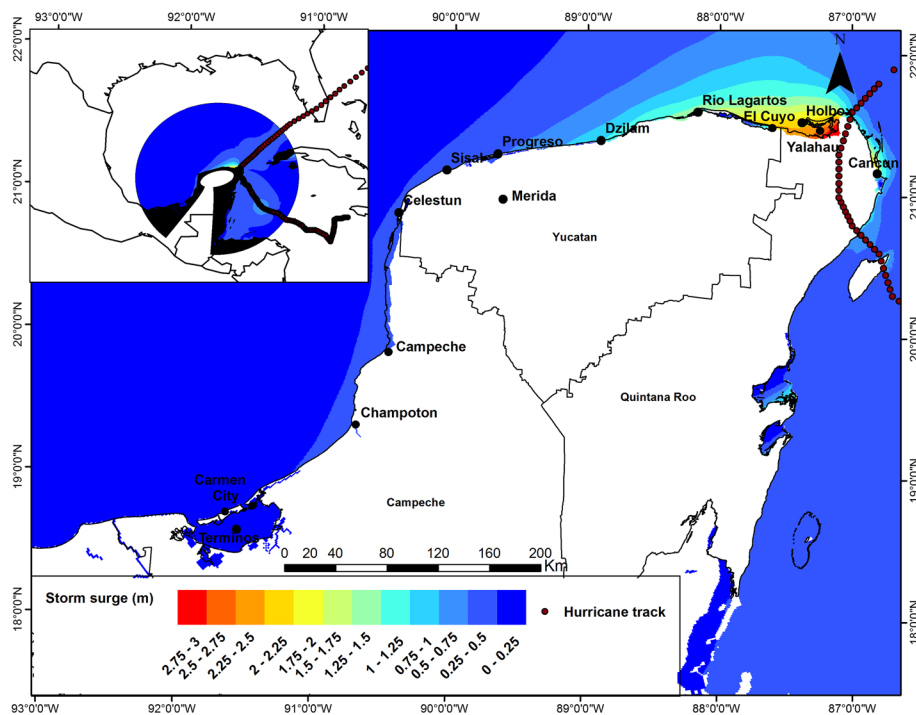

Fig. 5 Maximum Envelope of Water for Hurricane Wilma along the north-eastern part of the Yucatan Peninsula. The upper-left insert shows the trajectory of Hurricane Wilma and the SLOSH computational domain
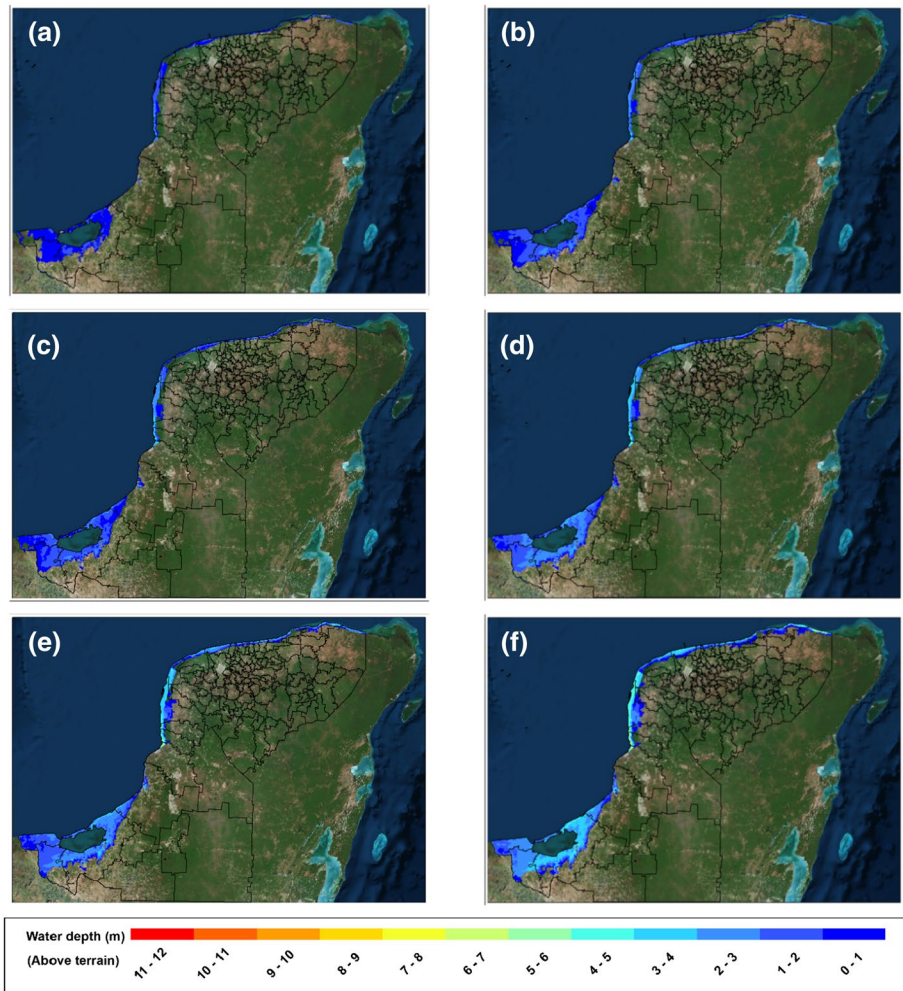
Fig. 6 Hurricane inundation (m) maps based on the SSHWS category tropical storm-II SLOSH MOMs product: **a**, **b** tropical storm, for low and high tide, respectively, **c**, **d** category I, for low and high tide, respectively, **e**, **f** category II, for low and high tide, respectively

1815 events. With the exception of the tropical storm category, all the storm parameters, direction of motion and tide anomaly were the same to create each MOM. Therefore, it is expected that when the wind intensity increases, the potential impact increases as well. The worst-case flood scenario occurred for the MOM associated with category-V hurricanes and high tide, which reached up to 12 m (Fig. 7f) around the Champoton area. These results may be related to the fact that storms propagating from north to south interact with the wide and flat continental shelf of the northern part of the Peninsula as well as the concave shape and low topography of areas surrounding Terminos lagoon and Champoton, and limitations of the SLOSH model, which will be mentioned in the discussion section. This physical vulnerability considerably increases the flooding threat. However, it should be stressed that the areas surrounding the Terminos lagoon
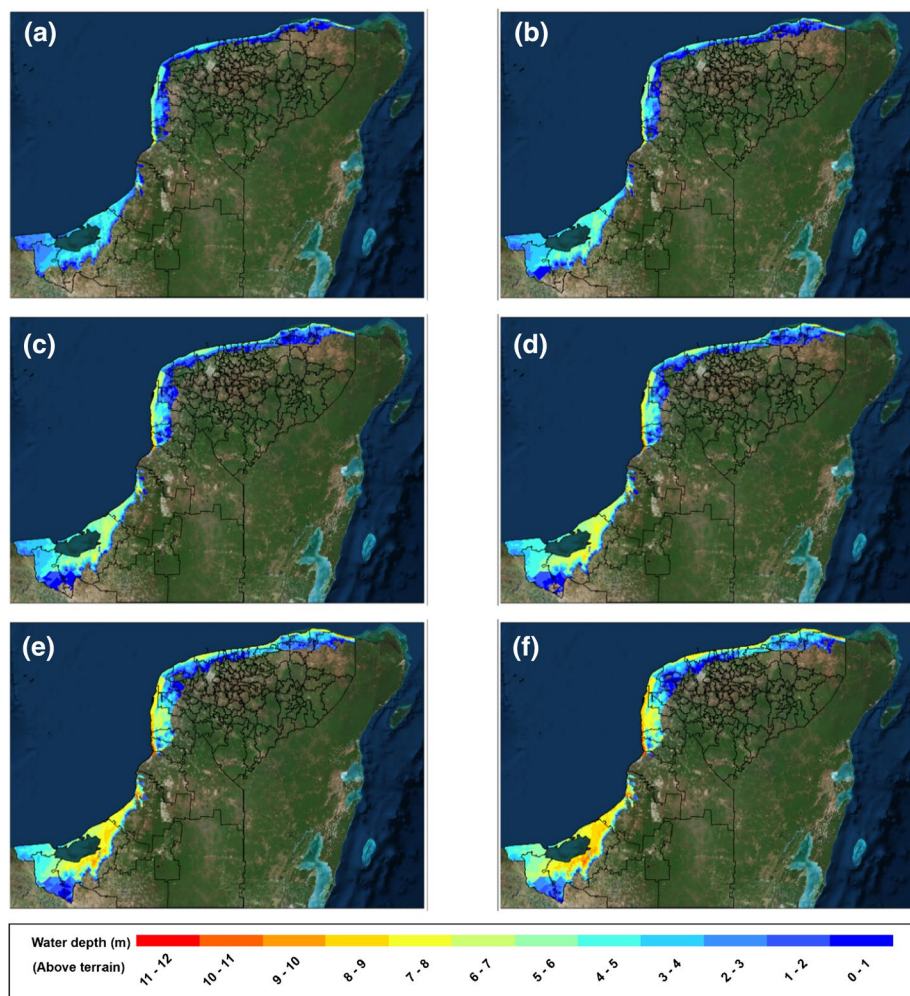
Fig. 7 Hurricane inundation (m) maps based on the SSHWS category 3 to 5 SLOSH MOMs product: **a**, **b** category III for low and high tide, respectively, (c)-(d) category IV, for low and high tide, respectively, **e**, **f** category V, for low and high, respectively

have the poorest grid cell resolution of the whole land area, around 1.3 km. The northern part of the Peninsula (Yucatan State) has the highest resolution (490–600 m). The highest hurricane storm surges on the northern part of the Peninsula occur when storm events come from the north, have a high category, low forward speed and are large in size. Even though these southward directions of motion are only possible when Nortes (southward cold fronts crossing the Gulf of Mexico) interact with TCs, as was the case for hurricanes Roxanne in 1955 and Isidore in 2002, storm surges from these events are part of the flood hazard spectrum and should therefore be considered in the flood hazard assessment. Since there are no historical flood observations available to validate the model, the uncertainty may be significant. These model results may be improved by further investigation once higher-resolution topography is available as well as better model setup (e.g., building a smaller computational domain to increase the spatial resolution in

flood-prone areas). Hence, results from this study should be seen as a first approximation for the study area.

At a worldwide level, according to the World Meteorological Organization (WMO), the largest recorded storm surge ever was 13 m (WMO 2006). This event is called the Bathurst Bay Hurricane, also known as Tropical Cyclone Mahina which occurred on March 5, 1899, near Bathurst Bay, northeast Australia (Nott et al. 2014). There are many approximations for the hurricane storm surge of this event, for instance Whittingham (1958) infers that the storm surge had a height of 43 (13.10 m) ft above mean sea level and extended 2–3 miles inland, fish and dolphins were reported found on top of 15-m-high cliffs. However, Nott et al. (2014) state that the wave action, wave setup and wave run-up were responsible for depositing the debris over the cliff tops. Based on this, they proposed a more reasonable estimation for the storm surge of Mahina of 30 ft (9 m) high. At a regional level, historical hurricane storm surges have been recorded with large values. For example, Hurricane Camile in 1969 reached up to 7.32 m in the Gulfport area, Mississippi (Jelesnianski et al. 1992). Hurricane Katrina in 2005 reached up to 7.6 m around Bay St. Louis, Mississippi (Lin et al. 2010). Therefore, in the context of these southward category-V storms hitting a concave coast as in Terminos or Champoton, the results reported here are reasonable.

Overall, the flood hazard increases with increasing hurricane category. Table 4 shows the size of the flooded areas for each MOM category for the low and high tide in the states of Yucatan and Campeche. As expected, the flooded area for the high tide is larger than that for low tide, due to the contribution of the astronomic tide level. Flooded area is defined in this study as: the area with topography with highs greater than zero and covered by ocean water. The hazard MOM maps show that the maximum expected flooded area occurs with the MOM for category V at high tide. Therefore, this MOM represents the maximum area susceptible to hurricane flooding. Based on this maximum flooded area (category V at high tide), a percentage of the maximum flooded area for each MOM was calculated.

4.2 Socioeconomic vulnerability

Figure 8 shows the socioeconomic vulnerability map for the study area. Merida (in red) stands out as the only municipality with very high vulnerability. Areas outside of the inundation threat (Fig. 7f) presented zero risk; areas where either the flood hazard or vulnerability is zero, the flood risk is zero. Most of the coastal municipalities in Yucatan show very low and low vulnerability with the exception of Tizimin (eastern part of Yucatan) with a high value. In contrast, Campeche presented high values along all of its coast. Undoubtedly, the resolution at the municipal level is a limitation for this study. Nevertheless, due

Table 4 Size of flooded areas and percentage of the maximum flooded area for each MOM category

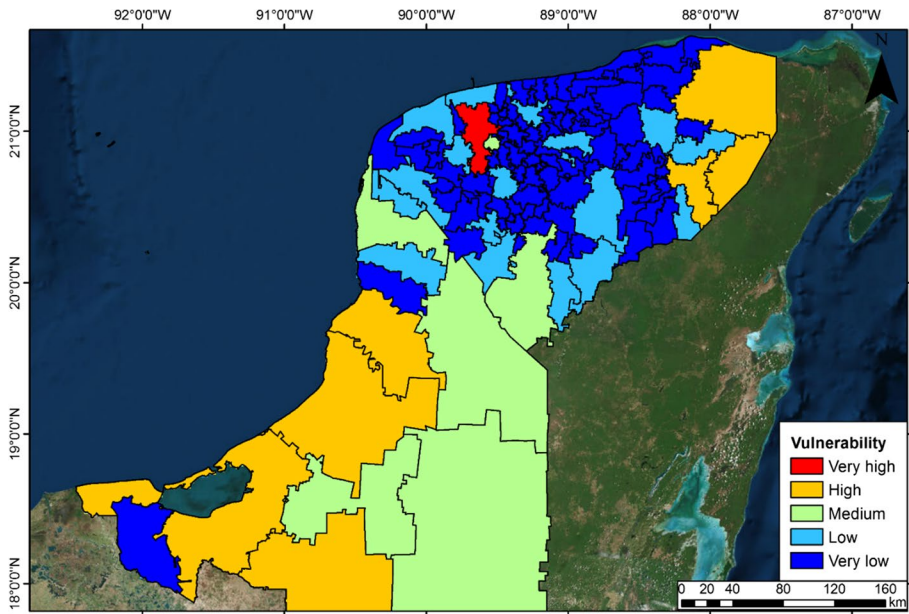| Hurricane category	Low tide	High tide
Tropical storm	5218.02 km^2 (28.17%)	7188.95 km^2 (38.81%)
Category 1	7251.83 km^2 (39.15%)	8269.90 km^2 (44.65%)
Category 2	8792.69 km^2 (47.46%)	10,257.86 km^2 (55.38%)
Category 3	12,200.72 km^2 (65.86%)	13,633.76 km^2 (73.60%)
Category 4	15,999.90 km^2 (86.37%)	16,815.79 km^2 (90.78%)
Category 5	17,992.48 km^2 (97.13%)	18,522.81 km^2 (100%)

Fig. 8 Socioeconomic vulnerability

to the scarcity of vulnerability data for some coastal towns, the municipality resolution was the best choice. It is a fact that the more people there are living close to the coastline, the more vulnerable these areas are (Dinh et al. 2012). Consequently, most of the Campeche municipalities, as well as the eastern part of Yucatan State, present high vulnerability (Fig. 8).

4.3 Flood risk

The flood risk levels are presented in Table 3, which are the results of the product of the hazard and vulnerability levels. Flood risk MOMs from tropical cyclone to category-II hurricane for low and high tide are presented in Fig. 9, and for category-III to category-V hurricanes in Fig. 10. These figures show that Campeche State generally has a higher flood risk than Yucatan. Usually flood risk is represented by a map in which the highest risk rank for each grid cell is considered. In this case, that map would be the one from Fig. 10 f. This aspect will be mentioned in the discussion section.

For MOMs associated with tropical storms and category-I hurricanes, the maximum flood risk category reached is high along parts of the Campeche coast and the east of Yucatan. For category-II hurricanes, there are some small areas with very high risk just north of the city of Campeche. For category-III to category-V MOMs, all five risk categories are presented in the study area. As mentioned above, areas with the highest risk are those with the most vulnerable population and where the highest water depth is reached, such as the areas surrounding Terminos lagoon, Champoton and the eastern part of the Yucatan State (Tizimin). Even though high water depths could be reached under several hurricane categories along the north-eastern part of the Yucatan state, the maximum risk
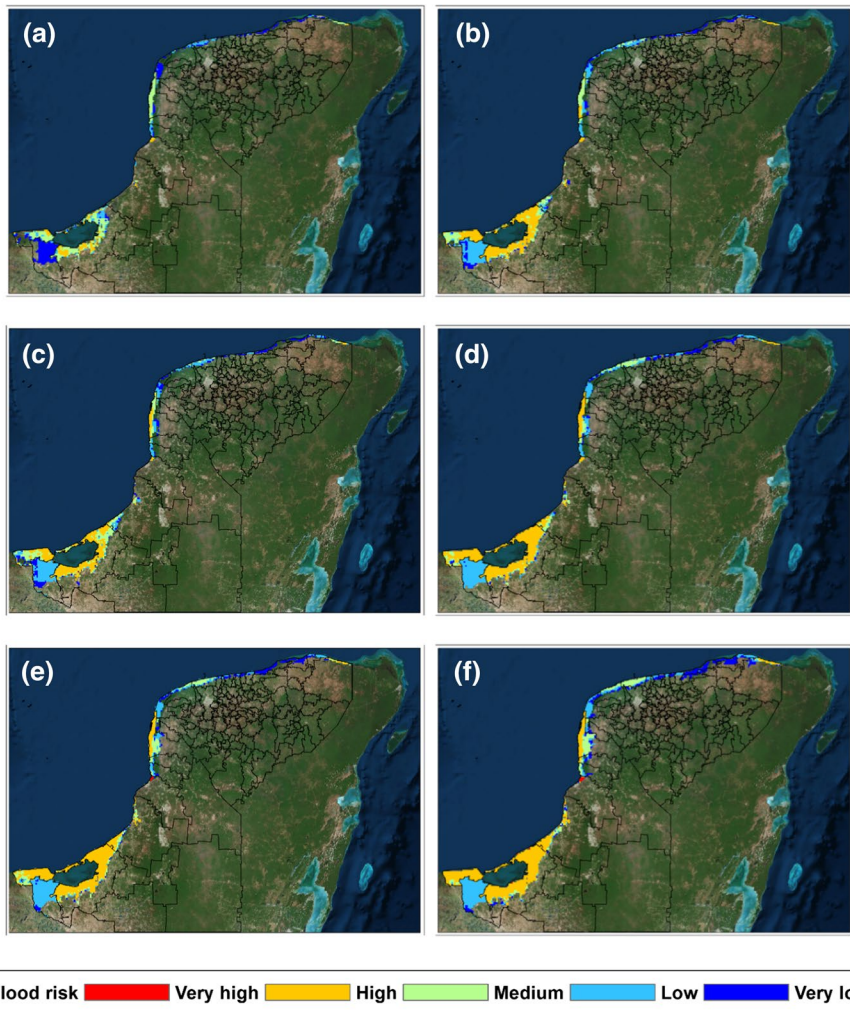
Fig. 9 Hurricane flood risk based on the SSHWS category tropical storm-II SLOSH MOMs product: **a**, **b** tropical storm, low and high tide, respectively, **c**, **d** category I, low and high tide, respectively, **e**, **f** category II, low and high tide, respectively

is medium due to very low vulnerability. Other municipalities with low vulnerability, for instance, Progreso and Hunucma (located in the northwest of Yucatan State), reached a high flood risk under MOMs associated with a high hurricane category. The Merida municipality, the only municipality with very high vulnerability, reaches flood risk categories from low to very high.

The flood risk map worst-case scenario (Fig. 10f) is the MOM associated with category-V hurricanes at high tide. The sizes of the areas belonging to this scenario for very low, low, medium, high and very high-risk zone areas are 2047.71, 3594.80, 3177.75, 5264.48 and 3599.39 km^2, corresponding to 11.58%, 20.33%, 17.97%, 29.77%, 20.35%, respectively. From this perspective, more than half of the studied area (50.12%) susceptible to hurricane flooding presents a high and very high risk.
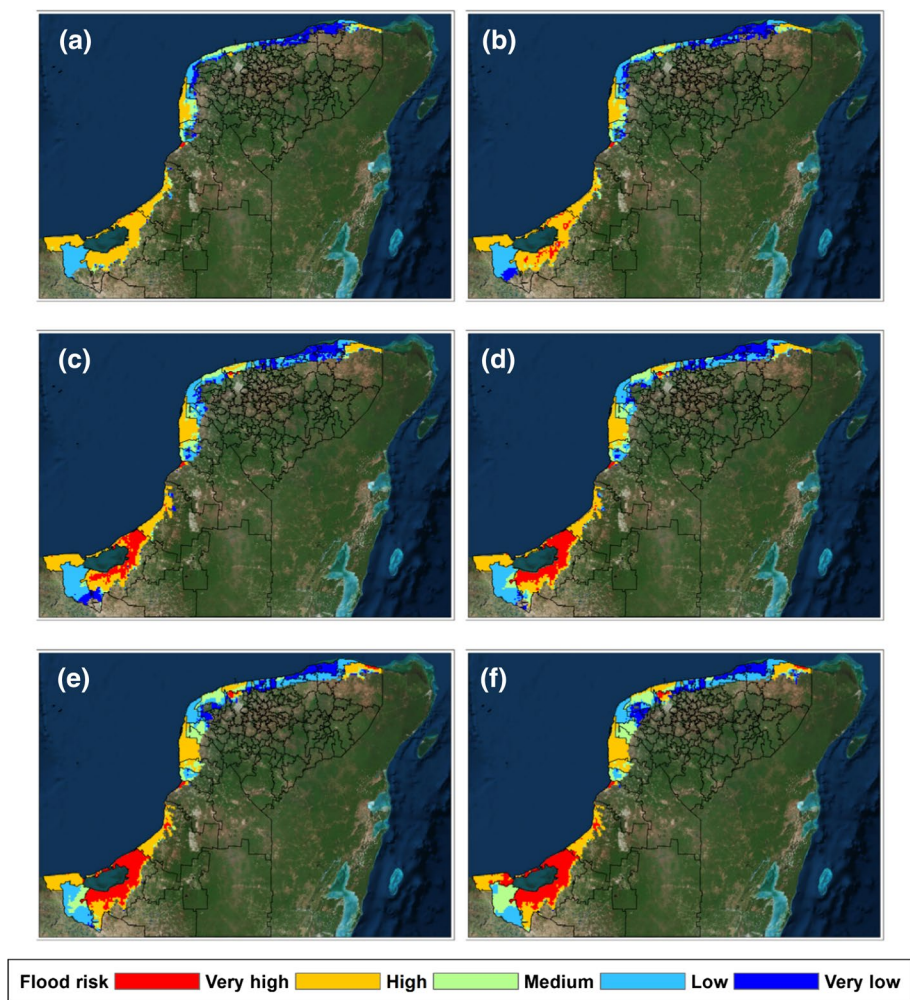
Fig. 10 Hurricane flood risk based on the SSHWS category 3 to 5 SLOSH MOMs product: **a, b** category III, low and high tide, respectively, **c, d** category IV, low and high tide, respectively, **e, f** category V, low and high tide, respectively

5 Discussion

This paper assessed the potential inundation threat and flood risk of TCs for the northern Yucatan Peninsula. The flood hazard of TCs was characterized by means of MEOWs and MOMs. In order to show the consequences of MOMs on society, urban development and the natural environment, these MOM maps for different TC categories and tide level were combined with the flood vulnerability map to obtain flood risk maps for each storm category and each tidal level (low or high).

Regarding the flood hazard characterization, the highest water depth was reached along the Campeche State coast, in particular at Terminos lagoon, partly because of its physical vulnerability (low-lying topography–bathymetry, Yucatan platform and concave

coastline). In the Yucatan State, the greatest water depth was reached along the northwest and east of the state, especially around areas with semi-enclosed back-barrier water bodies (lagoons, ports, wetlands). However, it is very important to take into account the limitations of the model in order to understand these results. The bottom friction of the SLOSH model does not include the effects of variation in land cover. This is an important drawback for the SLOSH model because land-cover friction has significant effects on inundation. For instance, the mangroves reduced water-level heights at rates of 4.2 and 9.4 cm/km along the Gulf coast of south Florida during Hurricanes Wilma and Charley, which occurred in 2004 and 2005, respectively (Krauss et al. 2009). Zhang et al. (2012), by means of the two-dimensional, finite-difference Coastal and Estuarine Storm Tide (CEST) model (Zhang et al. 2008), which solves the continuity and full momentum equations and zoned Manning coefficients, found that the surge inundation decreased in the heavily vegetated and highly developed areas because of increasing bottom friction. Through numerical experiments with the CEST model, these authors also found that the inundation area due to Wilma would extend more than 70% further inland without the mangrove zone along South Florida. Therefore, mangroves may support a protective role in reducing water levels associated with surges (Krauss et al. 2009).

Moreover, the use of linearized momentum equations in the SLOSH model can result in over-predictions in surge estimates. Zhang et al. (2008) carried out a numerical experiment using the CEST model and a hypothetical hurricane landfall at Miami, with and without nonlinear terms. The simulation results showed that maximum surges without nonlinear terms are about a foot higher than those with nonlinear terms. Therefore, neglecting the nonlinear terms can make a significant difference, in particular for small or mild storms where the storm surge can be in the order of this error. The issues related to the computational cost of including these nonlinear terms in the model have been solved with recent improvement in computer capabilities, although for operational models it may still be a problem.

Other limitation of the SLOSH model is the insufficient spatial resolution for computing overland flooding. In this study, the grid resolution for the western zone of the domain, i.e., in the vicinity of the city of Ciudad del Carmen, is too coarse (roughly 1.6 km) to resolve topographic features such as barrier islands and inlets in the low-lying area. This issue may be partially solved by building overlapping and smaller SLOSH grids than the one for this study to increase the resolution in areas of special interest, similar to the SLOSH basins for the East coast of the USA (Shaffer et al. 1989). Consequently, the predicted extent of the flooded area may be improved by increasing the grid resolution (Zhang et al. 2008).

Another factor that was not taken into account in this study was the contribution of wave setup to the water depth (Dorrestein 1961; Longuet-Higgins and Stewart 1963). By means of numerical modeling and synthetic hurricanes, Lin et al. (2012) found that the wave setup contribution is less than 1.5% of the surge for four locations around New York harbor. Furthermore, a recent numerical study for the northern Yucatan Peninsula found that wave setup ranged from 0.14 to 0.35 m during the pass of Central American cold surge events (Rey et al. 2018), but there are no studies for wave setup during the pass of TCs in this area. Therefore, further investigations are still needed once more data and strong computational power are available.

Undoubtedly, factors such as bottom friction, nonlinear terms and waves play an important role in storm surges. Therefore, all of these must be considered in future studies. Even though there are limitations regarding topographic data for the study area and for the model, this study represents the first approximation of the inundation threat and flood risk for the states of Yucatan and Campeche. Previous studies (Posada-Vanegas et al. 2011;

Meza-Padilla et al. 2015) have modeled the hurricane storm surge but not estimated hurricane floods and flood risk in the study area.

The methodology for computing MEOWs and MOMs is widely used and accepted in the USA. Consequently, this work represents a didactic tool that can be easily used on an international scale. On the other hand, the MEOWs may be used to forecast flooding when a storm makes landfall. Based on predicted storm characteristics, the MEOW with characteristics similar to those of the predicted storm may be used as an initial estimate of the flood-prone areas, which is useful for deciding which zones should be evacuated. The user must keep in mind that only a small portion of the coastline will experience the high flooding associated with a MEOW. This is because the MEOW's indicate the extend of possible flooding from tracks that are parallel to each other with the same category, forward speed and direction of motion, not the flooding from one individual storm (Shaffer et al. 1989). This information may be useful to emergency managers as civil protection measures.

Regarding the flood risk analysis, different maps for flood risk are presented, with one MOM determined for each. The map for the highest risk rank is the MOM map for hurricane category V and high tide, which is the worst-case scenario and usually used to apply flood protection measures. However, in this study, flood risk maps for different hurricane categories are presented, which may be useful for several applications in flood risk management, similar to the use of flood risk maps with associated return periods. In this study, no extreme analysis was performed; however, future research should be focused on associating return periods to MEOWs and MOMs, at least at the local level, by means of hydrodynamic modeling using synthetic hurricanes (Lin et al. 2010, 2014).

Even though there are evacuation plans for storm events in Mexico, the population does not usually evacuate. Consequently, there are not only economic losses but also fatal casualties. For instance, during Hurricane Isidore in 2002 around 980 people did not evacuate their houses in the eastern part of the Yucatan state. There are several reasons for this: i) looting activities when people leave their homes, ii) people distrusting the authorities, which are considered inefficient during contingency plans and iii) underestimation of the hurricane inundation threat. This is clear evidence of social and institutional vulnerability. However, the vulnerability estimation for this study takes into account aspects of mobility (age), education, household and access to information (Chen et al. 2013). These vulnerable aspects are easier to express in qualitative rather than in quantitative (money) form. The experience of hurricane Katrina, Rita and Ike in the USA has emphasized the significance of social influence because the impact of storms and floods was not only overlooked but also underestimated (IPET 2009; Cutter et al. 2013). In recent years, hurricanes Harvey and Irma caused severe damage and fatalities in the USA and the Caribbean Sea, suggesting that better science and decision making are necessary.

This study is the first approximation of hurricane flood risk in the states of Yucatan and Campeche. Since the spatial resolution for vulnerability indicators is coarser than the resolution for the flood hazard MOM, the flood risk spatial variability is more influenced by the spatial variation of the water depth. The flood risk estimation method used in this study is similar to the work on the Long Xuyen Quadrangle in Vietnam (Dinh et al. 2012), except for the socioeconomic indicators and hydrogeological vulnerability indicators. Flood risk maps at the regional level are useful to highlight areas that need more in-depth attention (Clark et al. 1998).

An increase in risk is not only because of a higher frequency of the hazard but also because of the vulnerability of society, which is connected to an increasing population, settlement placed in hazardous locations and increases in population density in urban areas (Komac et al. 2012). Natural disasters can occur where and when urban areas and natural

hazards meet in space and time (Alcántara-Ayala 2002). We do not have control over hazards, though we may have the ability to change the physical vulnerability of the coast by means of improving flood protection measures. There are two types of measures, non-structural and structural. Non-structural measures are those which do not involve physical construction but use knowledge, practice or agreement to reduce disaster risk and impacts, in particular through policies and laws, raising public awareness, training and education (UNISDR 2009). Structural measures are any physical construction used to reduce or avoid the possible impact of hazards (UNISDR 2009), such as dikes, embankments, spurs and levees which reduce the risk to a certain extent; however, these can never completely eliminate all the inundations since they are designed and constructed based on flood events from the past, thus can fail when larger floods occur (Plate 2002; Patro et al. 2009). The failure of dikes has caused some of the largest flood disasters in the world, for instance, the flood in the Yangtze river in China (Plate 2002), Hurricane Katrina in 2005 and 2011's Mississippi and Missouri River flooding (Cutter et al. 2013). Therefore, the application of non-structural measurements such as institutional policies, flood risk zoning based on flood modeling and flood forecasting is preferred (Patro et al. 2009; Dinh et al. 2012), since they offer additional tools for flood risk management.

6 Conclusions

This paper provides the first flood hazard and flood risk maps based on SLOSH MOM products associated with meteorological events ranging from tropical storms to category-V hurricanes in the states of Yucatan and Campeche. In order to improve the estimation of flood areas and flood risk, further investigation must take into account factors such as bottom friction, nonlinear terms, wave setup, as well as finer grids and improved coastal topographic and bathymetric data.

Results from this study can be useful for governments, insurance companies, coastal communities and policy makers to define adequate risk mitigation measures. While the flood hazard (MEOWs and MOMs) may be useful to emergency managers as civil protection measures, the flood risk would be an effective tool for flood risk management to implement flood protection initiatives.

Campeche State coast presents a higher flood risk than Yucatan State coast because its physical and socioeconomic vulnerability are higher. The city of Ciudad del Carmen presents the highest flood risk because of its geographical position, low-lying topography and concave coastal configuration. However, Campeche, as well as Yucatan towns such as Celestun, Hunucma, Progreso, and the east part of Yucatan are susceptible to flooding under MOM hurricane categories higher than II.

The SLOSH model results highlight the need for high-resolution topographic data along Mexican coastal areas, especially the eastern portion of the Yucatan Peninsula, in order to supply accurate storm surge modeling results.

References

Alcántara-Ayala I (2002) Geomorphology, natural hazards, vulnerability and prevention of natural disasters in developing countries. Geomorphology 47:107–124. https://doi.org/10.1016/S0169-555X(02)00083-1

Amante C, Eakins BW (2009) ETOPO1 1 arc-minute global relief model: procedures, data sources and analysis. In: NOAA technical memorandum NESDIS NGDC-24. National Hurricane Center, Boulder, p 19

Andersen OB (1995) Global ocean tides from ERS 1 and TOPEX/POSEIDON altimetry. J Geophys Res 100:25249–25259

Appendini CM, Hernández-Lasheras J, Meza-Padilla R, Kurczyn JA (2018) Effect of climate change on wind waves generated by anticyclonic cold front intrusions in the Gulf of Mexico. Clim Dyn 0:1–17. https://doi.org/10.1007/s00382-018-4108-4

Arakawa A, Lamb VR (1977) Computational design of the basic dynamical processes of the UCLA general circulation model. In: Chang J (ed) Methods of computational physics, vol 17. Academic Press, New York, Ny, USA, pp 173–265

Balica SF, Popescu I, Beevers L, Wright NG (2013) Parametric and physically based modelling techniques for flood risk and vulnerability assessment: a comparison. Environ Model Softw 41:84–92. https://doi.org/10.1016/j.envsoft.2012.11.002

Bronstert A (2003) Floods and climate change: interactions and impacts. Risk Anal 23:545–557. https://doi.org/10.1111/1539-6924.00335

Cenapred (2006) Guía básica para la elaboración de atlas estatales y municipales de peligros y riesgo: Fenómenos hidrometeorológicos. Secretaría de Gobernación, México, D.F., p 140

Chen W, Cutter SL, Emrich CT, Shi P (2013) Measuring social vulnerability to natural hazards in the Yangtze River Delta region, China. Int J Disaster Risk Sci 4:169–181. https://doi.org/10.1007/s13753-013-0018-6

Chen J, Chen J, Liao A et al (2015) Global land cover mapping at 30 m resolution: a POK-based operational approach. ISPRS J Photogramm Remote Sens 103:7–27. https://doi.org/10.1016/j.isprsjprs.2014.09.002

Chowdhury JU, Karim MF (1996) A risk-based zoning of storm surge prone area of the Ganges Tidal plans. J Civ Eng Inst Eng Bangladesh 24:221–233

Clark GE, Moser SC, Ratick SJ et al (1998) Assessing the vulnerability of coastal communities to extreme storms: the case of revere, MA, USA. Mitig Adapt Strateg Glob Change 3:59–82

Cuevas-Jiménez A, Euán-Ávila J (2009) Morphodynamics of carbonate beaches in the Yucatán Peninsula. Ciencias Mar 35:307–319

Cutter SL, Barnes L, Berry M et al (2008) A place-based model for understanding community resilience to natural disasters. Glob Environ Change 18:598–606. https://doi.org/10.1016/j.gloenvcha.2008.07.013

Cutter SL, Emrich CT, Morath DP, Dunning CM (2013) Integrating social vulnerability into federal flood risk management planning. J Flood Risk Manag 6:332–344. https://doi.org/10.1111/jfr3.12018

DHI (2014) Mike 21 flow model FM: hydrodynamic module, user guide. DHI Water & Environment, Hoersholm, p 134

Di Risio M, Bruschi A, Lisi I et al (2017) Comparative analysis of coastal flooding vulnerability and hazard assessment at national scale. J Mar Sci Eng 5:51. https://doi.org/10.3390/jmse5040051

Dinh Q, Balica S, Popescu I, Jonoski A (2012) Climate change impact on flood hazard, vulnerability and risk of the Long Xuyen Quadrangle in the Mekong Delta Climate change impact on flood hazard, vulnerability and risk of the Long Xuyen. Int J River Basin Manag 10:103–120. https://doi.org/10.1080/15715124.2012.663383

Dorrestein R (1961) Wave set-up on a beach. In: Proceedings of 2nd technical conference on Hurricanes, Miami Beach, FL. National Hurricane Research Project 50. US Department of Commerce, pp 230–241

DY (1988) El Diario de Yucatan. Copies from 16 to 30 of September. Yucatanense Library, Merida

Emanuel K (2005) Increasing destructiveness of tropical cyclones over the past 30 years. Nature 436:686–688. https://doi.org/10.1038/nature03906

Emanuel K, Ravela S, Vivant E, Risi C (2006) A statistical deterministic approach to hurricane risk assessment. Bull Am Meteorol Soc 87:299–314. https://doi.org/10.1175/BAMS-87-3-299

Emanuel K, Sundararajan R, Williams J (2008) Hurricanes and global warming: results from downscaling IPCC AR4 simulations. Bull Am Meteorol Soc 89:347–367. https://doi.org/10.1175/BAMS-89-3-347

Fernandez P, Mourato S, Moreira M (2016) Social vulnerability assessment of flood risk using GIS-based multicriteria decision analysis. A case study of Vila Nova de Gaia (Portugal). Geomat Nat Hazards Risk 7:1367–1389. https://doi.org/10.1080/19475705.2015.1052021

Flather RA (2001) Storm Surges. In: Steele JH, Thorpe SA, Turekian KK (eds) Encyclopedia of ocean sciences. Academic, San Diego, pp 2882–2892

Forbes C, Rhome J, Mattocks C, Taylor A (2014) Predicting the storm surge threat of hurricane sandy with the national weather service SLOSH model. Mar Sci Eng 2:437–476. https://doi.org/10.3390/jmse2020437

Gallopín GC (2006) Linkages between vulnerability, resilience, and adaptive capacity. Glob Environ Change 16:293–303. https://doi.org/10.1016/j.gloenvcha.2006.02.004

INEGI (2010) Censo de Población y Vivienda 2010. In: INEGI. http://www.beta.inegi.org.mx/proyectos/ccpv/2010/. Accessed 25 May 2017

IPET (2009) Performance evaluation of the New Orleans and Southeast Louisiana hurricane protection system, vol 1. Executive summary and overview. US Army Corps of Engineers, Washington, DC

Jarvinen BR, Neumann CJ, Davis MAS (1984) A tropical cyclone data tape for the North Atlantic basin, 1886–1983: contents, limitations, and uses. In: NOAA Technical Memo NWS NHC 22. Miami, Fla. National Hurricane Center, p 21

Jelesnianski CP (1970) "Bottom stress time-history" in linearized equations of motion for storm surges. Mon Weather Rev 98:462–478

Jelesnianski C, Chen J, Shaffer W (1992) SLOSH: sea, lake, and overland surges from hurricanes. NOAA Technical Report NWS 48, United States Department Commerce NOAA/AOML Library, Miami

Jelesniansky CP (1967) Numerical computations of storm surges with bottom stress. Mon Weather Rev 95:740–756. https://doi.org/10.1175/1520-0493(1967)095%3c0740:NCOSSW%3e2.3.CO;2

Jenks GF (1963) Generalization in statistical mapping. Ann As Am Geogr 53:15–26. https://doi.org/10.1111/j.1467-8306.1963.tb00429.x

Kim SC, Chen J (1999) Bottom stress of wind-driven currents over an inner shelf determined from depth-integrated storm surge model. J Coast Res 15:766–773

Knutson TR (2015) Tropical cyclones and hurricanes|Tropical cyclones and climate change, 2nd edn. Elsevier, Amsterdam

Knutson TR, McBride JL, Chan J et al (2010) Tropical cyclones and climate change. Nat Geosci 3:157–163. https://doi.org/10.1038/ngeo779

Komac B, Zorn M, Kušar D (2012) New possibilities for assessing the damage caused by natural disasters in Slovenia—the case of the Real Estate Record. Geogr Vestn 84:113–127

Krauss KW, Doyle TW, Doyle TJ et al (2009) Water level observations in mangrove swamps during two hurricanes in Florida. Wetlands 29:142–149. https://doi.org/10.1672/07-232.1

Lin N, Chavas D (2012) On hurricane parametric wind and applications in storm surge modeling. J Geophys Res Atmos 117:1–19. https://doi.org/10.1029/2011JD017126

Lin N, Emanuel KA, Smith JA, Vanmarcke E (2010) Risk assessment of hurricane storm surge for New York City. J Geophys Res 115:1–11. https://doi.org/10.1029/2009JD013630

Lin N, Emanuel K, Oppenheimer M, Vanmarcke E (2012) Physically based assessment of hurricane surge threat under climate change. Nat Clim Change 2:462–467. https://doi.org/10.1038/NCLIMATE1389

Lin N, Lane P, Emanuel KA et al (2014) Heightened hurricane surge risk in northwest Florida revealed from climatological-hydrodynamic modeling and paleorecord reconstruction. J Geophys Res Atmos 119:8606–8623. https://doi.org/10.1002/2014JD021584

Longuet-Higgins MS, Stewart R (1963) A note on wave set-up. J Mar Res 21:4–10

Martínez-Graña AM, Boski T, Goy JL et al (2016) Coastal-flood risk management in central Algarve: vulnerability and flood risk indices (South Portugal). Ecol Indic 71:302–316. https://doi.org/10.1016/j.ecolind.2016.07.021

Massey WG, Gangai JW, Drei-Horgan E, Slover KJ (2007) History of coastal inundation models. Mar Technol Soc J 41:7–17. https://doi.org/10.4031/002533207787442303

Merz B, Thieken AH, Gocht M (2007) Flood risk mapping at the local scale: concepts and challenges. In: Begum S, Stive MJF, Hall J (eds) Advances in natural and technological hazards research. Springer, Dordrecht, pp 231–251

Merz B, Hall J, Disse M, Schumann A (2010) Fluvial flood risk management in a changing world. Nat Hazards Earth Syst Sci 10:509–527

Meza-Padilla R, Appendini CM, Pedrozo-Acuña A (2015) Hurricane-induced waves and storm surge modeling for the Mexican coast. Ocean Dyn 65:1199–1211. https://doi.org/10.1007/s10236-015-0861-7

Morrow BH, Lazo JK, Rhome J, Feyen J (2015) Improving storm surge risk communication: stakeholder perspectives. Bull Am Meteorol Soc 96:35–48. https://doi.org/10.1175/BAMS-D-13-00197.1

Nageswara Rao K, Subraelu P, Rao TV et al (2008) Sea-level rise and coastal vulnerability: an assessment of Andhra Pradesh coast, India through remote sensing and GIS. J Coast Conserv 12:195–207. https://doi.org/10.1007/s11852-009-0042-2

NHC (2014a) Storm surge overview. http://www.nhc.noaa.gov/surge/. Accessed 5 May 2017

NHC (2014b) Storm surge maximum envelope of water (MEOW). http://www.nhc.noaa.gov/surge/meowOverview.php. Accessed 5 May 2017

NHC (2014c) Storm surge maximum of the maximum (MOM). http://www.nhc.noaa.gov/surge/momOverview.php. Accessed 5 May 2017

Nkwunonwo U, Whitworth M, Baily B (2015) Relevance of social vulnerability assessment to flood risk reduction in the Lagos Metropolis of Nigeria. Br J Appl Sci Technol 8:366–382. https://doi.org/10.9734/BJAST/2015/17518

Nott J, Green C, Townsend I, Callaghan J (2014) The world record storm surge and the most intense southern hemisphere tropical cyclone: new evidence and modeling. Bull Am Meteorol Soc 95:757–765. https://doi.org/10.1175/BAMS-D-12-00233.1

Ojeda E, Appendini CM, Mendoza ET (2017) Storm-wave trends in Mexican waters of the Gulf of Mexico and Caribbean Sea. Nat Hazards Earth Syst Sci 17:1305–1317. https://doi.org/10.5194/nhess-17-1305-2017

Patro S, Chatterjee C, Mohanty S et al (2009) Flood inundation modeling using MIKE FLOOD and remote sensing data. J Indian Soc Remote Sens 37:107–118. https://doi.org/10.1007/s12524-009-0002-1

Penning-Rowsell E, Fordham M, Correia F et al (1994) Flood hazard assessment, modelling and management: results from the EUROflood project. In: Penning-Rowsell E, Fordham M (eds) Floods across Europe: flood hazard assessment, modelling and management. University Press, London, pp 37–72

Plate EEJ (2002) Flood risk and flood management. J Hydrol 267:2–11. https://doi.org/10.1016/S0022-1694(02)00135-X

Platzman G (1963) The dynamic prediction of wind tides on Lake Erie. Meteorol Monogr Am Meteorol Soc 4:44

Posada-Vanegas G, Durán-Valdez G, Silva-Casarin R et al (2011) Vulnerability to coastal flooding induced by tropical cyclones. In: Smith JM, Lynett P (eds) Coastal engineering proceedings. Shanghai, China, p 14

Rey W, Salles P, Mendoza ET et al (2018) Assessment of coastal flooding and associated hydrodynamic processes on the Southeast coast of Mexico, during Central American Cold Surge events. Nat Hazards Earth Syst Sci 18:1681–1701. https://doi.org/10.5194/nhess-2017-64

Rosengaus-Moshinsky M, Jiménez-Espinosa M, Vázquez-Conde MT (2002) Atlas climatológico de ciclones tropicales en México. Centro Nacional de Prevención de Desastres, Instituto Mexicano de Tecnología del Agua, Ciudad de México, p 108

Ruol P, Martinelli L, Favaretto C (2018) Vulnerability analysis of the venetian littoral and adopted mitigation strategy. Water 10:984. https://doi.org/10.3390/w10080984

Shaffer WA, Jelesniansky CP, Chen J (1989) Hurricane storm surge forecasting. In: Preprints, 11th conference on probability and statistics on atmospheric science. American Meteorology Society, Monterrey, pp 53–58

Silva SF, Martinho M, Capitão R et al (2017) An index-based method for coastal-flood risk assessment in low-lying areas (Costa de Caparica, Portugal). Ocean Coast Manag 144:90–104. https://doi.org/10.1016/j.ocecoaman.2017.04.010

Sleigh PA, Gaskell PH, Berzins M, Wright NG (1998) An unstructured finite volume algorithm for predicting flow in rivers and estuaries. Comput Fluids 27:479–508. https://doi.org/10.1016/S0045-7930(97)00071-6

Stringfield VT, LeGrand HE (1974) Karst hydrology of Northern Yucatan Peninsula, Mexico. In: Weidie AE (ed) Proceedings of field seminar on water and carbonate rocks of the Yucatan Peninsula, Mexico. New Orleans Geological Society, New Orleans, pp 192–210

Taylor A, Glahn B (2008) Probabilistic guidance for hurricane storm surge. In: Proceedings of the 88th annual meeting of the American Meteorological Society, New Orleans, pp 1–8

Taylor A, Myckow A, Fritz A, et al (2013) Recent developments in probabilistic hurricane storm surge (P-Surge 2.0). In: Proceedings of the estuarine and coastal modeling conference XIII, ECM13, San Diego

Tingsanchali T, Karim MF (2005) Flood hazard and risk analysis in the southwest region of Bangladesh. Hydrol Process 19:2055–2069. https://doi.org/10.1002/hyp.5666

UNISDR (2009) UNISDR-terminology on disaster risk reduction. UNISDR, Geneva, p 30

Whittingham H (1958) The Bathurst Bay Hurricane and associated storm surge. Aust Met Mag 23:14–36

Wind HG, Nierop TM, De Blois CJ, De Kok JL (1999) Analysis of flood damages from the 1993 and 1995 Meuse floods. Water Resour Res 35:3459–3465. https://doi.org/10.1029/1999WR900192

WMO (2006) World meteorological organization's world weather and climate extremes archive. https://wmo.asu.edu/. Accessed 19 May 2017

Zachry BC, Booth WJ, Rhome JR, Sharon TM (2015) A national view of storm surge risk and inundation. Weather Clim Soc 7:109–117. https://doi.org/10.1175/WCAS-D-14-00049.1

Zhang K, Xiao C, Shen J (2008) Comparison of the CEST and SLOSH models for storm surge flooding comparison of the CEST and SLOSH models for storm. J Coast Res 24:489–499. https://doi.org/10.2112/06-0709.1

Zhang K, Liu H, Li Y et al (2012) The role of mangroves in attenuating storm surges. Estuar Coast Shelf Sci 102–103:11–23. https://doi.org/10.1016/j.ecss.2012.02.021

Zhang K, Li Y, Liu H et al (2013) Transition of the coastal and estuarine storm tide model to an operational storm surge forecast model: a case study of the Florida Coast. Weather Forecast 28:1019–1037. https://doi.org/10.1175/WAF-D-12-00076.1

Zhao DH, Shen HW, Tabios GQ et al (1994) Finite-volume two-dimensional unsteady-flow model for River Basins. J Hydraul Eng 120:863–883. https://doi.org/10.1061/(ASCE)0733-9429(1994)120:12(1497)

Affiliations

Wilmer Rey[1,2] · **E. Tonatiuh Mendoza[2,3]** · **Paulo Salles[2,3]** · **Keqi Zhang[4]** ·
Yi-Chen Teng[5,6] · **Miguel A. Trejo-Rangel[2]** · **Gemma L. Franklin[2,3]**

[1] Dirección General Marítima, Centro de Investigaciones Oceanográficas e Hidrográficas del Caribe, Barrio Bosque, Sector Manzanillo Escuela Naval, Cartagena de Indias, Colombia

[2] Laboratorio de Ingeniería y Procesos Costeros, Instituto de Ingeniería, UNAM, Puerto de Abrigo S/N, 92718 Sisal, Mexico

[3] Laboratorio Nacional de Resiliencia Costera, CONACyT, Mérida, Yucatán, Mexico

[4] International Hurricane Research Center, Florida International University, Miami, FL 33199, USA

[5] Graduate Institute of Hydrological and Oceanic Sciences, National Central University, Taoyuan, Taiwan

[6] Michael Baker International, Hamilton, NJ, USA